The role of kinetic effects, including plasma rotation and energetic particles, in resistive wall mode stability[a]

J. W. Berkery,[1,b] S. A. Sabbagh,[1] H. Reimerdes,[1] R. Betti,[2] B. Hu,[2] R. E. Bell,[2]
S. P. Gerhardt,[3] J. Manickam,[3] and M. Podestà[3]

[1]*Department of Applied Physics and Applied Mathematics, Columbia University, New York,
New York 10027, USA*
[2]*Laboratory for Laser Energetics, University of Rochester, Rochester, New York 14623, USA*
[3]*Princeton Plasma Physics Laboratory, Princeton University, Princeton, New Jersey 08543, USA*

The resistive wall mode (RWM) instability in high-beta tokamaks is stabilized by energy dissipation mechanisms that depend on plasma rotation and kinetic effects. Kinetic modification of ideal stability calculated with the "MISK" code [B. Hu *et al.*, Phys. Plasmas **12**, 057301 (2005)] is outlined. For an advanced scenario ITER [R. Aymar *et al.*, Nucl. Fusion **41**, 1301 (2001)] plasma, the present calculation finds that alpha particles are required for RWM stability at presently expected levels of plasma rotation. Kinetic stabilization theory is tested in an experiment in the National Spherical Torus Experiment (NSTX) [M. Ono *et al.*, Nucl. Fusion **40**, 557 (2000)] that produced marginally stable plasmas with various energetic particle contents. Plasmas with the highest and lowest energetic particle content agree with calculations predicting that increased energetic particle pressure is stabilizing but does not alter the nonmonotonic dependence of stability on plasma rotation due to thermal particle resonances. Presently, the full MISK model, including thermal particles and an isotropic slowing-down distribution function for energetic particles, overpredicts stability in NSTX experiments. Minor alteration of either effect in the theory may yield agreement; several possibilities are discussed. © *2010 American Institute of Physics*. [doi:10.1063/1.3474925]

I. INTRODUCTION

Toroidal magnetic confinement fusion devices can suffer from instabilities of the plasma equilibrium that lead to the disruption of the plasma current and discharge termination. When the plasma pressure in such devices is raised above a certain level, a kinking of the magnetic field lines theoretically becomes unstable and grows exponentially. The presence of a resistive wall in close proximity to the plasma edge acts to slow the growth of this mode considerably, to the time scale of the penetration of field through the wall τ_w, but the wall itself does not stabilize this resistive wall mode (RWM).[1] Fusion plasmas can operate with the ratio of plasma pressure to magnetic pressure β above the "no-wall" stability limit,[2,3] however. An explanation of this passive stability of high β plasmas to the RWM is needed for confident extrapolation to future devices. Effects which either dissipate the energy of the mode or provide a force that resists the displacement of field should be considered. In the present work, we considered the role of kinetic effects in RWM stability, including the effects of resonances between the plasma rotation and thermal particle frequencies and the restorative force effect of energetic particles.

Classic theoretical models of RWM stabilization through energy dissipation predicted a "critical" plasma toroidal rotation sufficient to stabilize the mode.[4] This critical rotation has traditionally been characterized by a scalar fraction of the Alfvén frequency at the $q=2$ surface of the order of 1%.[5,6] In the National Spherical Torus Experiment (NSTX),[7] however, the RWM can become unstable with a wide range of rotation profiles[8,9] or it can remain stable to very low rotation levels. Figure 1 shows an equilibrium with high plasma rotation that is stable, which is subsequently slowed by $n=3$ nonresonant magnetic braking[10] to the intermediate profile that is unstable to the RWM. Some shots, however, make it through this intermediate rotation and remain stable down to very low rotation (Fig. 1). A theoretical model broad enough to explain these results is needed.

The kinetic effects of thermal particles on the stability of RWMs in NSTX have been previously explored.[8,9] Here, we extend that analysis to include the effects of energetic particles. Examples of energetic particles are fast ions from either neutral beam injection or high energy alpha particles resulting from fusion reactions. In general, the interaction of energetic particles with plasma instabilities can lead to stabilizing *or* destabilizing effects.[11,12] Alpha particles have been theoretically shown to make an important contribution to the kinetic stability of the RWM (Ref. 13) and internal kink mode[14] in ITER.[15] Calculations with the "MARS-K" code of the RWM stability of a DIII-D equilibrium indicate that beam ions can have a large effect on stability.[16] In NSTX, we find that energetic particles are generally stabilizing and that a reduction of this particle population leads to reduced RWM stability. A correlation between energetic particle modes and RWM destabilization has been observed in JT-60U.[17] It is well known that energetic particle-induced modes, such as
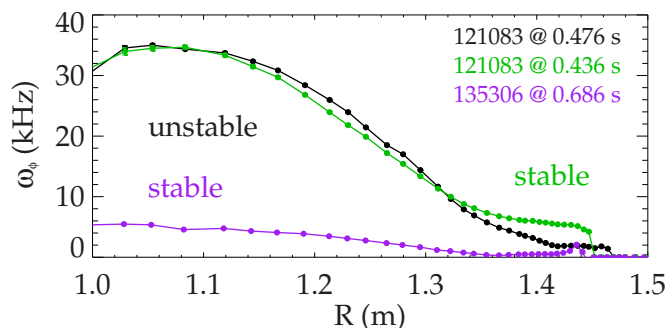

FIG. 1. (Color online) Toroidal plasma rotation profiles for NSTX, showing a high rotation stable case, an intermediate rotation unstable case, and a low rotation stable case.
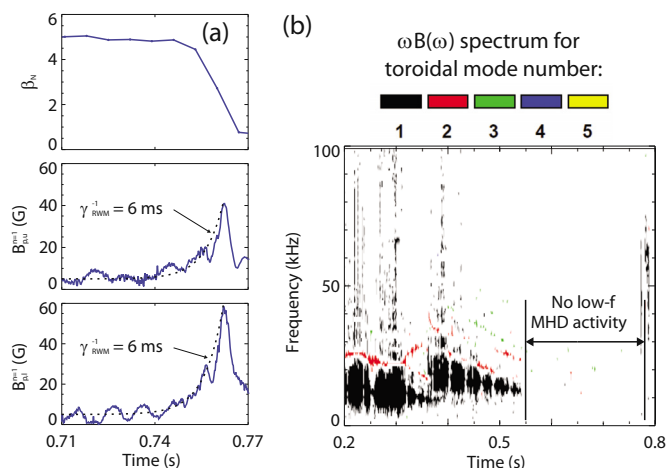

FIG. 2. (Color online) Time traces for NSTX shot 130235: (a) β_N; amplitude of $n=1$ poloidal field perturbation from upper and lower RWM sensors and (b) MHD activity spectrogram.

Alfvén eigenmodes, can lead to a loss or redistribution of the energetic particle population.[18] Therefore, a natural hypothesis arises that if the energetic particles that stabilize the RWM are lost by other mode activities, this loss might lead to RWM destabilization. This mechanism might explain the energetic particle mode "triggering" of RWMs in JT-60U and help substantiate the larger hypothesis and theory of RWM stabilization by energetic particles.

In this paper, we explored the effect of energetic particles on RWM stability by changing the energetic particle content in marginally stable NSTX plasmas and then examining their predicted stability through kinetic stabilization theory. This theory and the numerical codes that use it, such as the "MISK" code,[13] have been updated to include the kinetic effects of energetic particles. Because of their high energy, which yields larger precession drift and bounce frequencies and lower collision frequencies, and because of their different distribution function, energetic particles have a different interaction with the mode than thermal particles do.

In Sec. II, the experimental characteristics of a RWM in NSTX are briefly presented. In Sec. III, we reviewed kinetic RWM stabilization theory, arriving at a general form for the perturbed potential energy due to kinetic effects, δW_K, in terms of the distribution function of the particles considered—a Maxwellian for thermal particles or an isotropic slowing-down distribution function for energetic particles. This approach is highlighted in Sec. IV by an example showing the effect of plasma rotation and alpha particles on RWM stability in ITER and a comparison between theoretical prediction and experimental results in NSTX. Section V discusses changes to the model that may enable a better quantitative agreement between the MISK calculation and experimental measurements.

II. RWM EXPERIMENTAL CHARACTERISTICS

Unstable RWM characteristics in low aspect ratio NSTX plasmas have been documented and are briefly summarized, with specifics for recent discharges illustrated here. Without active feedback control, the growing $n=1$ RWM is typically stationary in the laboratory frame,[19] but occasionally exhibits a period of slow toroidal rotation (rotation frequency of $\sim 1/\tau_w$) before terminating the plasma.[3] The RWM is identified in NSTX by a variety of observations. Foremost is a

growing signal on low frequency poloidal magnetic sensors located between the plasma and the vacuum vessel. Figure 2(a) shows the $n=1$ RWM amplitude, analyzed from two arrays of 12 sensor signals above and below the midplane, growing exponentially with a time scale $\gamma_{RWM}^{-1} \approx 6$ ms. The present experiments, aimed to study RWM marginal stability, targeted plasma configurations and conditions for which low-order tearing modes are stable. This is verified during RWM growth by ultrasoft x-ray signals that show a global collapse in magnitude, while their phase does not show an inversion that would indicate a tearing mode.[9] A plot of the magneto-hydrodynamic (MHD) mode spectrum from a toroidal array of magnetic pickup loops [Fig. 2(b)] further shows no rotating mode activity, indicative of a saturated tearing instability leading up to the time of RWM instability. In this case, the plasma was driven unstable by an intentional change in plasma rotation profile caused by the applied $n=3$ magnetic braking fields. Once the RWM grows sufficiently, as in this case, the plasma β and the plasma current are disrupted and the discharge terminates due to the unstable mode. Plasmas reaching marginal RWM stability in this paper are defined by the equilibria that occur just before the observed instability appears. Note that active RWM control has been demonstrated in NSTX (Ref. 20) by maintaining a sufficiently low $n=1$ RWM amplitude, greatly reducing the probability of plasma disruption, while allowing plasma toroidal rotation to spin the mode faster than $1/\tau_w$, thereby converting the RMW to a rotating kink/ballooning mode that is strongly damped in the presence of the stabilizing plates.[8]

III. KINETIC THEORY OF RWM STABILITY

The energy principle for resistive wall modes neglecting plasma inertia and kinetic effects can be written[21] as

$$\gamma \tau_w = -\delta W_\infty / \delta W_b, \tag{1}$$

where δW_∞ is the sum of the plasma fluid and vacuum perturbed potential energies when the wall is placed at infinity and δW_b is the sum of the plasma fluid and vacuum δWs when the wall is placed at a specific location b. The above

expression is valid in the range when $\beta_\infty < \beta < \beta_b$, that is, when beta is above the no-wall limit, but below the ideal "with-wall" limit. In the above equation, γ is the growth rate of the resistive wall mode.

When kinetic effects are included, the RWM dispersion relation takes the form[13,22–24]

$$(\gamma - i\omega_r)\tau_w = -\frac{\delta W_\infty + \delta W_K}{\delta W_b + \delta W_K},$$ (2)

where the kinetic contribution, δW_K, has both real and imaginary parts and ω_r is the mode rotation frequency.

The change in the potential energy of a plasma equilibrium due to kinetic effects can be written (in terms of the plasma displacement eigenfunction) as

$$\delta W_K = -\frac{1}{2}\int \boldsymbol{\xi}_\perp^* \cdot (\boldsymbol{\nabla} \cdot \widetilde{\mathbb{P}}_K)d\mathbf{V}.$$ (3)

The perturbed kinetic pressure tensor, $\widetilde{\mathbb{P}}_K$, is found by taking a moment of the perturbed distribution function, which results from the solution of the linearized, bounce-averaged drift kinetic equation. Substituting velocity and volume integrals with integrals over particle energy, ε, pitch angle, $\chi = v_\parallel/v$, and magnetic flux, Ψ, we arrive at a general expression for δW_K in terms of the distribution function, f_j, of the particles j considered

$$\delta W_K = \frac{\sqrt{2}\pi^2}{m_j^{3/2}}\sum_{l=-\infty}^{\infty}\int d\varepsilon \int d\chi \int \frac{d\Psi}{B_0}\hat{\tau}\left(-2|\chi|\frac{B_0}{B}\right)$$

$$\times \frac{(\omega_r + i\gamma - \omega_E)\frac{\partial f_j}{\partial \varepsilon} - \frac{1}{eZ_j}\frac{\partial f_j}{\partial \Psi}}{\langle \omega_D^j \rangle + l\omega_b^j - i\nu_{\mathrm{eff}}^j + \omega_E - \omega_r - i\gamma}\varepsilon^{5/2}|\langle H/\hat{\varepsilon}\rangle|^2.$$ (4)

One can see that δW_K depends on $\partial f/\partial \varepsilon$ and $\partial f/\partial \Psi$. Here, $H/\hat{\varepsilon}$ and $\hat{\tau}$ are given by Eqs. (12) and (13) of Ref. 14, and the first four frequencies in the denominator are the precession drift, bounce, collision, and $E \times B$ frequencies, respectively. Summation over all bounce harmonics, l, is included, but in practice $|l| > 4$ makes δW_K negligibly small. Radial force balance, neglecting poloidal rotation, implies that $\omega_E = \omega_\phi - \omega_{*i}$, where ω_ϕ is the plasma toroidal rotation frequency and ω_{*i} is the ion diamagnetic frequency. The above expression is for trapped particles. For circulating particles, similar expressions can also be derived.

Note that previously,[9] δW_K had been formulated in terms of $\Sigma_{\pm\sigma}\int d\Lambda$ instead of $\int(-2|\chi|B_0/B)d\chi$, where $\sigma = \mathrm{sgn}(v_\parallel)$ and $\Lambda = B_0/B(1 - \chi^2)$. That formulation had forced f to be symmetric about $\chi = 0$, but that restriction is lifted in Eq. (4). This will be important for future consideration of energetic particles with anisotropic distribution functions.

A. Thermal particles: Maxwellian distribution function

Using a Maxwellian distribution function in Eq. (4) leads to the familiar form of δW_K for trapped thermal particles, as in Eq. (8) of Ref. 14. The contribution to RWM stabilization in NSTX from thermal particles, including trapped thermal ions and electrons and circulating thermal ions, has been previously considered in detail.[8,9] Resonances

between thermal particle (primarily trapped ion) precession drift or bounce frequencies and the Doppler-shifted mode rotation frequency provide the kinetic dissipation of energy that can help stabilize the RWM. This stabilization will be discussed further in the context of ITER and NSTX analysis in Sec. IV.

B. Energetic particles: Slowing-down distribution function

Energetic particles provide both a fluid contribution to the pressure that is typically destabilizing and a stabilizing kinetic contribution similar to the one described by Van Dam et al.[25] in the limits of large diamagnetic and precession drift frequencies. For thermal particles, the Doppler-shifted mode frequency, $\omega_E - \omega_r$, can resonate with $\langle \omega_D \rangle$ or ω_b in the denominator of Eq. (4), causing δW_K to be large and complex.[9] However, $\omega_D \propto \varepsilon$ and $\omega_b \propto \sqrt{\varepsilon}$, so for energetic particles ω_D, $\omega_b \gg \omega_E$. Therefore, energetic particles are not in an energy dissipation mode-particle resonance, and the contribution to δW_K from energetic particles is mostly real and approximately independent of ω_ϕ. In the absence of drift reversal, the kinetic effects of energetic particles are stabilizing and have been shown to suppress the internal kink.[26] In this paper, we considered the ideal plasma resistive wall mode that generates a perturbation in the plasma similar to an ideal kink/ballooning mode. The modes are related to a characteristic difference that the RWM eigenfunction is necessarily coupled to the conducting structure of the device. The stabilizing effect of energetic particles on the RWM is therefore similar to that examined for the internal kink. It is a real restorative force that arises from conservation of magnetic flux enclosed by precessional drift orbits when ω_D is large.[26] In other words, energetic particles make the magnetic flux more rigid and resistant to change by the RWM. Similarly, research that has examined various physical effects (e.g., rotation shear, passing particle effects, and anisotropy) on internal kink stabilization[27,28] is applicable to the RWM. A typical difference for neutral beam heated plasmas is that the differential rotation between the plasma and the mode is large for the RWM and is small for the internal kink, which changes the evaluation of stabilizing resonances. In the MISK code, both fluid and kinetic contributions are included and the overall effect is found to be stabilizing for the RWM. These results are also consistent with those of Hu et al. for both the RWM (Ref. 13) and the internal kink.[14]

We will now choose a simple isotropic form for f for energetic particles that facilitates straightforward calculation of δW_K with the MISK code, but other forms of $f(\varepsilon, \chi, \Psi)$ could be used in Eq. (4) as well, so long as they provide smooth derivatives $\partial f/\partial \varepsilon$ and $\partial f/\partial \Psi$. We will return to this point in Sec. III B 2.

For trapped energetic ions, a simple Lorentzian slowing-down distribution function has the form[16]

$$f_a(\varepsilon, \Psi) = \frac{3n_a}{8\sqrt{2}\pi}[\ln(1 + \hat{\varepsilon}_c^{-3/2})]^{-1}\frac{(m_a/\varepsilon_a)^{3/2}}{\hat{\varepsilon}^{3/2} + \hat{\varepsilon}_c^{3/2}}$$ (5)

for ε up to the maximum energy, ε_a. Here, $\hat{\varepsilon} = \varepsilon/\varepsilon_a$ and

$$\hat{\varepsilon}_c = \left(\frac{3\sqrt{\pi}}{4}\right)^{2/3}\left(\frac{m_a}{m_i}\right)\left(\frac{m_i}{m_e}\right)^{1/3}\left(\frac{T_e}{\varepsilon_a}\right). \tag{6}$$

Note that the subscript a will be used throughout this paper to represent energetic particles, in general, and later α will be used, more specifically, for alpha particles.

Substitution of Eq. (5) into Eq. (4) results in

$$\delta W_K^a = \frac{\pi}{4}\sum_{l=-\infty}^{\infty}\int d\hat{\varepsilon}\int d\chi\int \frac{d\Psi}{B_0}n_a\varepsilon_a\hat{\tau}^a\left(2|\chi|\frac{B_0}{B}\right)\left(\int \frac{\hat{\varepsilon}^{1/2}}{\hat{\varepsilon}^{3/2}+\hat{\varepsilon}_c^{3/2}}d\hat{\varepsilon}\right)^{-1}\frac{\hat{\varepsilon}^{5/2}}{\hat{\varepsilon}^{3/2}+\hat{\varepsilon}_c^{3/2}}|\langle H/\hat{\varepsilon}\rangle|^2$$

$$\times\left[\frac{\frac{3}{2}\hat{\varepsilon}^{1/2}}{\hat{\varepsilon}^{3/2}+\hat{\varepsilon}_c^{3/2}}(\omega_E-\omega_r-i\gamma)+\frac{\varepsilon_a}{eZ_a}\left(\frac{1}{\hat{\varepsilon}^{3/2}+\hat{\varepsilon}_c^{3/2}}\frac{d\hat{\varepsilon}_c^{3/2}}{d\Psi}-\frac{1}{n_a}\frac{\partial n_a}{\partial\Psi}-\omega_f^a\right)\right](\langle\omega_D^a\rangle+l\omega_b^a-i\nu_{\rm eff}^a+\omega_E-\omega_r-i\gamma)^{-1}. \tag{7}$$

Equation (7) is the same as Eq. (19) of Ref. 14, but integrated over χ instead of Λ, and with the addition of collisionality, $\nu_{\rm eff}^a$ (usually negligible for energetic particles), bounce frequency, and summation over l. Also,

$$\omega_f^a = \left(\int \frac{\hat{\varepsilon}^{1/2}}{\hat{\varepsilon}^{3/2}+\hat{\varepsilon}_c^{3/2}}d\hat{\varepsilon}\right)\frac{d}{d\Psi}\left[\left(\int \frac{\hat{\varepsilon}^{1/2}}{\hat{\varepsilon}^{3/2}+\hat{\varepsilon}_c^{3/2}}d\hat{\varepsilon}\right)^{-1}\right]. \tag{8}$$

The relationship between p_a, n_a, and ε_a for this distribution function is through Eq. (6) and the following:

$$p_a = \int f_a\left(\frac{2}{3}\varepsilon\right)d^3\mathbf{v}$$
$$= \varepsilon_a n_a\frac{2}{3}\left(\int \frac{\hat{\varepsilon}^{3/2}}{\hat{\varepsilon}^{3/2}+\hat{\varepsilon}_c^{3/2}}d\hat{\varepsilon}\right)\left(\int \frac{\hat{\varepsilon}^{1/2}}{\hat{\varepsilon}^{3/2}+\hat{\varepsilon}_c^{3/2}}d\hat{\varepsilon}\right)^{-1}, \tag{9}$$

as in Ref. 16. One must specify two of these three unknowns. Presently, two types of energetic particles will be considered: alpha particles and beam ions.

1. Alpha particles

In burning plasmas, alpha particles are important contributors to the plasma beta. For alpha particles, $\varepsilon_\alpha = 3.52$ MeV everywhere, by definition, and the distribution is isotropic with respect to pitch angle, so Eq. (5) is a good representation for f_α. Then a balance of the alpha particle production and slowing-down rates defines the alpha particle density profile[14]

$$n_\alpha = c_\alpha\tau_s\langle\sigma v\rangle n_e^2/4. \tag{10}$$

Therefore, ε_α and n_α are specified, and p_α is obtained from Eq. (9). The alpha pressure profile is then integrated over the volume to find β_α. In the above equation, c_α is an adjustable constant used to obtain the desired $\beta_\alpha/\beta_{\rm tot}$ for testing in the model. Note that the above balance contains some implicit simplifications (such as $n_D = n_T = n_e/2$) that can affect the calculated magnitude of n_α.[29] Also, the alpha particle pressure is subtracted from the total equilibrium pressure to obtain the thermal pressure, which is used in the calculations of the thermal components of δW_K.

2. Beam ions

In present day machines, energetic particles are typically supplied by neutral beams. Instead of using a simple balance such as Eq. (10), for beam ions n_a and p_a, profiles are specified as inputs to MISK. Then, Eqs. (6) and (9) are used to find ε_a, which is now a function of Ψ rather than a constant, and is not allowed to be larger than the neutral beam input energy. For example, the profiles of hot ion density and pressure shown in Figs. 3(a) and 3(b) were obtained from "TRANSP" (Ref. 30) for NSTX plasma 121090 @ 0.601 s. The calculated ε_a is shown in Fig. 3(c).

The isotropic slowing-down distribution function used [Eq. (5)] is accurate for fusion alpha particles but is not consistent with expectation and the internal model of TRANSP for beam ions. However, by using the density and pressure profiles from TRANSP, first order properties, such as β_a and the total stored energy in beam ions, are consistent. Efforts to
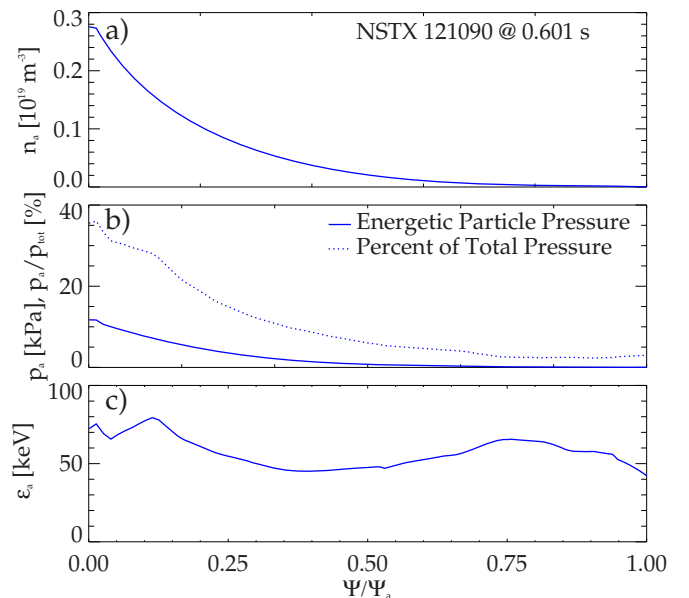

FIG. 3. (Color online) Energetic particle density (a) and pressure (b) profiles for an example shot from NSTX as calculated by TRANSP. Also shown in frame (b) in the dashed line is $p_a/p_{\rm tot}$. Frame (c) shows the characteristic energy of the slowing-down distribution function of Eq. (5), ε_a, as calculated from the above n_a and p_a profiles.
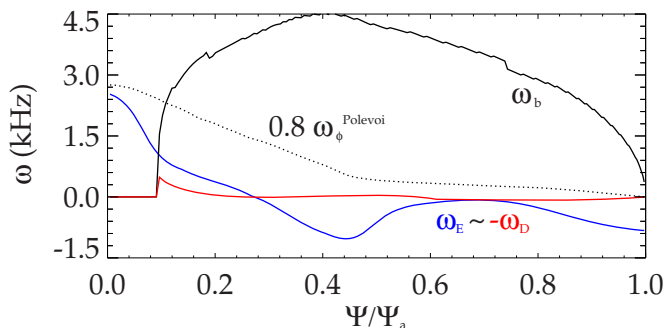
FIG. 4. (Color online) Profiles of 0.8 $\omega_\phi^{\text{Polevoi}}$, the resulting ω_E, ω_b with $\chi=0$ and $\hat{\varepsilon}=2$, and $-\langle\omega_D\rangle$ with $\chi=0$ and $\hat{\varepsilon}=\frac{3}{2}$ (see Ref. 9) vs Ψ for ITER scenario 4.
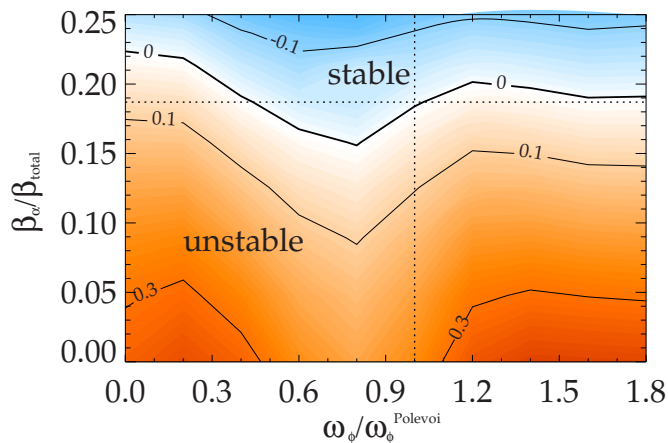

FIG. 5. (Color online) Contours of predicted $\gamma\tau_w$ vs the fraction of total β in α particles and scaled rotation for ITER scenario 4. The horizontal dashed line indicates the predicted $\beta_\alpha/\beta_{\text{tot}}$, while the vertical line indicates the $\omega_\phi^{\text{Polevoi}}$ profile.

include the effects of beam ion anisotropy will be discussed further in Sec. IV B 2.

IV. CALCULATION WITH THE MISK CODE

The ideal δW contributions to the energy principle [Eq. (2)] have been theoretically developed for years.[21] In the present work, NSTX experimental equilibria calculated with "EFIT" (Ref. 31) are input to "PEST,"[32] which is used to calculate the ideal terms and provide input to MISK. MISK has been previously used to calculate δW_K for NSTX cases without energetic particles.[8,9] For trapped thermal ions, this calculation follows Eq. (4), with f taken to be Maxwellian. Also included are trapped electrons and circulating thermal ions, with analogous equations that differ somewhat in detail,[14,33] and Alfvén layers at the rational surfaces that are treated separately and analytically. Here, we extend that calculation to include trapped energetic ions with a slowing-down f, as was discussed in Sec. III.

A. ITER

The stability of the RWM in ITER, including the kinetic effects of thermal particles, was previously calculated with the MARS-K code[33] and with both thermal and alpha particles using the MISK code.[13] Here, we have updated the MISK calculation to operate on the present ITER scenario 4 equilibrium with $\beta_N=2.96$ (above the $n=1$ no-wall ideal MHD stability limit, $\beta_{N,\text{no-wall}}^{n=1}=2.5$), and we explored the dependence of stability on energetic particles by scaling $\beta_\alpha/\beta_{\text{tot}}$, and on rotation by scaling ω_ϕ. The ω_ϕ profile is taken from Polevoi *et al.*[34]

1. The effect of plasma rotation

Figure 4 shows a representative scaled plasma rotation profile $(\omega_\phi/\omega_\phi^{\text{Polevoi}}=0.8)$ and the resulting ω_E profile, compared to representative ω_b and $-\langle\omega_D\rangle$ profiles for thermal ions. When the plasma rotation is 0.8 times the value of Polevoi *et al.*, ω_E and $-\langle\omega_D\rangle$ are in resonance over the range of $0.6<\Psi/\Psi_a<0.8$. This causes the denominator of Eq. (4) to be reduced, leading to higher δW_K. Therefore, we should expect to see increased stability with this rotation level. This is illustrated in Fig. 5, which shows the contours of MISK calculated RWM growth rates for this ITER scenario 4 equi-

librium on a plot of $\beta_\alpha/\beta_{\text{tot}}$ from 0 to 0.25 versus $\omega_\phi/\omega_\phi^{\text{Polevoi}}$. Included in this calculation are the effects of Alfvén layers at the rational surfaces, circulating thermal ions, and trapped electrons, thermal ions, and alpha particles. Using Eq. (10) with $c_\alpha=1$ and n_e, T_e, and T_i from the ITER scenario 4 equilibrium, we find that the expected $\beta_\alpha/\beta_{\text{tot}}$ $=0.187$. The effect of alpha particle pressure on RWM growth rate will be discussed in the next subsection, but to see the effect of rotation on stability, we can look at a horizontal slice at $\beta_\alpha/\beta_{\text{tot}}=0.187$. Here, we see the precession drift resonant stabilization centered at $\omega_\phi/\omega_\phi^{\text{Polevoi}}=0.8$. Similar stabilization is seen in NSTX at low rotation.[9] Below $\omega_\phi/\omega_\phi^{\text{Polevoi}}=0.8$, the resulting ω_E is lower and therefore between the stabilizing precession drift and $l=1$ bounce resonances, while above 0.8, ω_E is higher and between the precession drift and $l=-1$ bounce resonances (see Fig. 4).

We have also performed calculations for ITER scenario 4 equilibria with linear rotation profiles of the form ω_ϕ $=\omega_0(1-\Psi/\Psi_a)$. This analysis was done to make connection with the previous work that examined earlier ITER equilibria, also with alpha particles.[13] Qualitatively similar behavior was observed in that case, with intermediate rotation stability in between low and high rotation instability. Using the same linear profiles here, we have also obtained similar results to the $\omega_\phi/\omega_\phi^{\text{Polevoi}}$ case, although the maximum stability at $\beta_\alpha/\beta_{\text{tot}}=0.187$ was greater, with $\gamma\tau_w=-0.14$ rather than -0.05. In addition, MARS-K was recently used to examine the role of rotation in ITER stability, using both perturbative and self-consistent methods and using the same rotation frequency profile as that of Polevoi *et al.*, but without including alpha particles.[33] In that study, however, ω_E was scaled, as opposed to ω_ϕ here, which makes a direct comparison difficult. We can note, however, that as $\omega_E\to0$ in the MARS-K case, predicted stability increases, which is consistent with the picture presented here, in Fig. 4, that the ω_ϕ profile that causes $\omega_E\sim-\langle\omega_D\rangle$ (over a portion of the profile) increases stability.

2. The effect of energetic particles

In addition to scaling the expected rotation level, we can now explore the effect of alpha particles on ITER RWM stability by using c_α to scale $\beta_\alpha / \beta_{tot}$ in MISK. Figure 5 indicates that a sufficient population of alpha particles is required to stabilize the RWM for this ITER equilibrium at plasma rotation speeds from 0 to 1.8 times that predicted by Polevoi *et al.* Without any alpha particles, the plasma is predicted to be unstable regardless of the rotation. As the alpha particle β is increased, the growth rate decreases, eventually passing into a stable region. Above 23% alpha particle β, the calculation predicts that the plasma is *stable* to the RWM regardless of the rotation level. At the expected level of $\beta_\alpha / \beta_{tot} = 0.187$, this ITER equilibrium is predicted to just attain marginal stability with $\omega_\phi = \omega_\phi^{Polevoi}$ (Fig. 5). Note that adding alpha particles is stabilizing at any rotation level and does not affect the thermal particle precession drift resonant stabilization that occurs at $\omega_\phi / \omega_\phi^{Polevoi} = 0.8$, as discussed above. Presently, only thermal and alpha particles are considered in this analysis. ITER beam ions should be included in future studies, as they may be important as well.[35]

B. NSTX

Dedicated experiments were conducted in NSTX to examine the predictions of the kinetic model of RWM stability applied to ITER in the previous section. Here, we again examined the effect of plasma rotation and energetic particles in the context of that model.

1. The effect of plasma rotation

NSTX discharges with intermediate rotation profiles can have weakened stability to the RWM due to those profiles being in-between the stabilizing precession drift and bounce frequency resonances in kinetic theory.[9] Kinetic theory can also explain why high rotation *and* low rotation discharges in NSTX can be stable to the RWM. Figure 1 shows an example of each of these cases. In Fig. 6, we compare the ω_E profiles (calculated from ω_ϕ) for these two cases to the precession drift and bounce frequency profiles for thermal ions calculated from experimental data.[9] The high rotation case [Fig. 1(a)] has $\omega_E \approx \omega_b$ over the outer half of the flux surfaces. This means that the mode is in resonance with the $l = -1$ bounce harmonic of the thermal ions, which dissipates the energy of the mode, keeping it stable. Mathematically, in the denominator of Eq. (4), $\omega_E - \omega_b \approx 0$, leading to large δW_K. In the low rotation case [Fig. 1(b)], the mode is in stabilizing resonance with the precession drift frequency ($\omega_E \approx -\langle \omega_D \rangle$) of the thermal ions.

2. The effect of energetic particles

In a dedicated experiment, a series of discharges was performed in NSTX where the plasma current and magnetic field were scaled over a wide range, but their ratio was kept constant (therefore keeping the q profile roughly constant, with the objective of maintaining the same ideal plasma stability). Altering the confining field by changing I_p scanned
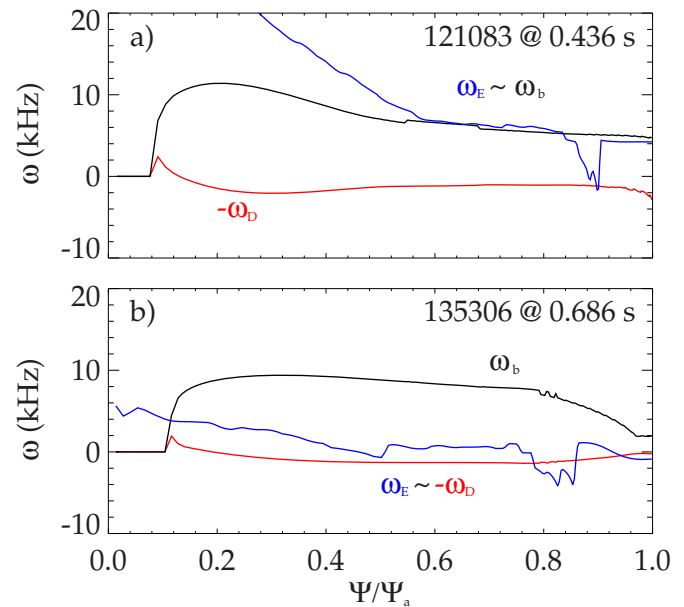

FIG. 6. (Color online) Comparison of frequency profiles vs normalized Ψ for two shots from NSTX: (a) with high rotation stability and (b) low rotation stability.

the confinement of energetic particles in the plasma, and therefore the equilibrium energetic particle density.

The fast ion D-alpha (FIDA) diagnostic for NSTX (Ref. 36) measures part of the distribution and gives relative density profiles of the energetic particles. Unfortunately, FIDA has an increasing signal to noise ratio as the plasma density increases during the shot, necessitating analysis early in the shot rather than the preferred time just before the unstable RWM that terminates the discharge. Despite these limitations, however, the FIDA results shown in Fig. 7(a) show that a change from $I_p = 0.8$ to 1.1 MA in these plasmas made a significant difference in the energetic particle density. The TRANSP computed p_a profiles in Fig. 7(b) show a similar trend to the FIDA measurements. The discharges from the
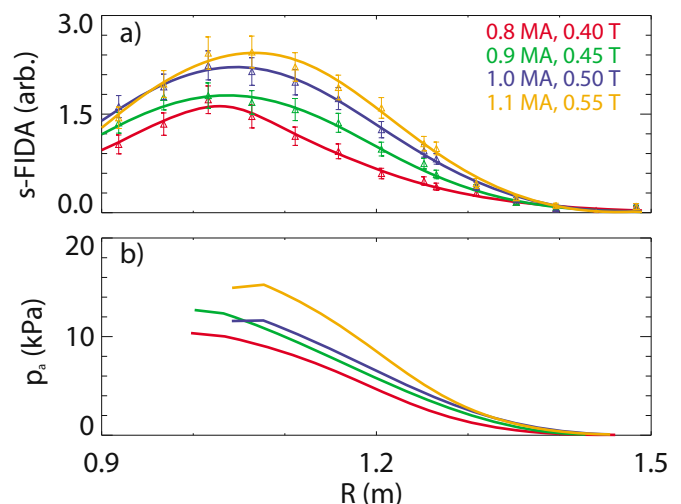

FIG. 7. (Color online) (a) FIDA signal vs radius at the midplane for several shots at different plasma current and magnetic field, in the time range of 0.22–0.25 s. (b) TRANSP fast ion pressure profiles for the same shots at the same times.
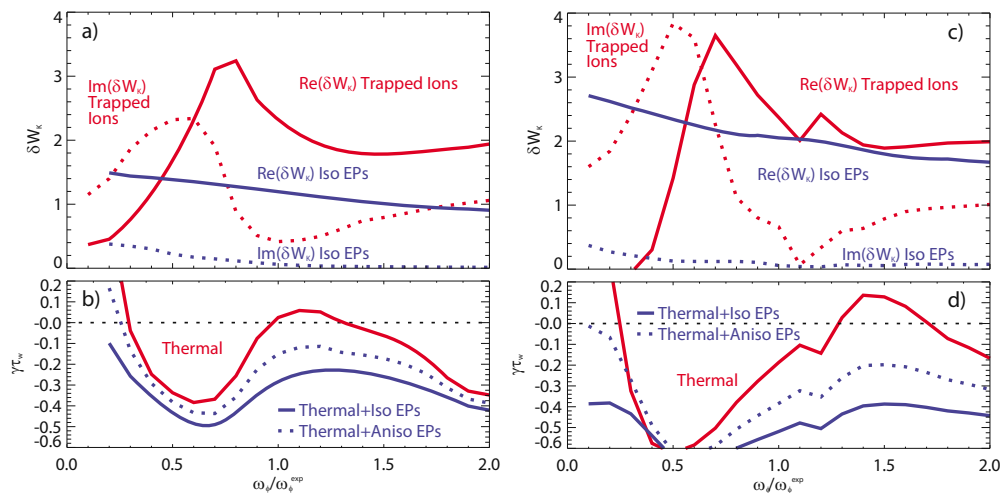
FIG. 8. (Color online) (a) MISK calculated real and imaginary δW_K for trapped thermal ions and for trapped energetic ions vs scaled experimental plasma rotation for NSTX shot 121083 @ 0.475 s ($\beta_a/\beta_{\text{tot}}=0.176$), and (b) the resulting normalized growth rates with and without including energetic particles in the calculation. The lower solid line is for isotropic beam ions, while the dashed line is for a simple model of anisotropic beam ions with a lower trapped fraction. (c) and (d) are the analogous plots for NSTX shot 121088 @ 0.460 s ($\beta_a/\beta_{\text{tot}}=0.312$).

scan of energetic particle pressure shown in Fig. 7 (and others) translate into a range of $\beta_a/\beta_{\text{tot}}$ of 17%–31% computed by "TRANSP" just before the unstable RWM.

For each condition, unstable RWMs were found by slowing the plasma rotation to the correct range for instability with $n=3$ nonresonant magnetic braking.[10] These RWMs were identified and diagnosed in the manner described in Sec. II.

In the present theoretical model, energetic particles add an additional stabilizing term to $\gamma\tau_w$ but they do not shift the range of the plasma rotation resulting in weakened stability, as was discussed in Sec. III B and will be shown in the following figures. Figure 8(a) shows the contribution to δW_K as a function of scaled experimental plasma rotation for thermal trapped ions compared to energetic trapped ions for NSTX shot 121083 @ 0.475 s, which has a $\beta_a/\beta_{\text{tot}}=0.176$, according to TRANSP. This shot experimentally goes unstable at this time, so $\omega_\phi^{\text{expt}}$ is the marginally stable rotation profile. As expected, the contribution from energetic particles is significant and mostly real, but is nearly independent of ω_ϕ, as opposed to the obvious resonances displayed in the thermal ion traces. As discussed in Sec. III B, $\omega_\phi \sim \omega_D$, ω_b for thermal particles, but $\omega_\phi \ll \omega_D$, ω_b for energetic particles. The slight decrease of δW_K with ω_ϕ for energetic particles is due to the slowly increasing importance of the ω_ϕ term in the denominator of Eq. (7) (ω_ϕ also appears in the numerator, but its influence there is comparatively smaller).

The effect of adding energetic particles to the calculation is to decrease the growth rate, as seen in Fig. 8(b). At the experimental rotation, the predicted growth rate goes from near zero to $\gamma\tau_w \approx -0.25$ when isotropic energetic particles are included. The predicted stabilizing effect of energetic particles, in addition to being nearly independent of rotation and collisionality, roughly scales with the energetic particle pressure. Figures 8(c) and 8(d) show the analogous plots for NSTX shot 121088 @ 0.460 s, which has a higher $\beta_a/\beta_{\text{tot}}$ of

0.312. The contribution to $\text{Re}(\delta W_K)$ from the energetic particles is correspondingly larger, and $\gamma\tau_w$ at the experimental rotation is reduced by -0.4.

The computed result showing that isotropic energetic particles add significant stabilizing effect is seemingly at odds with what is observed in experiments—namely, that unstable RWMs can be found in discharges with a wide range of $\beta_a/\beta_{\text{tot}}$. We are now investigating improvements to the present model that will bring quantitative agreement with experiments (an agreement between the observation of an unstable RWM for a certain plasma equilibrium and the calculation of a zero or slightly positive predicted growth rate for that equilibrium). We start by examining the effect of switching to a more realistic anisotropic distribution function.

Presently, only trapped beam ions with an isotropic distribution are considered. The isotropic beam ions are spread evenly across pitch angle, so that if χ_s (between 0 and 1) is the separatrix pitch angle between trapped and circulating ions, then the trapped beam ion fraction is simply equal to χ_s. If we instead considered an anisotropic distribution function directly from TRANSP (Ref. 37) or one with an analytical Gaussian form[35] $f_b(\varepsilon,\Psi,\chi)=f_a(\varepsilon,\Psi)C(\varepsilon,\Psi)e^{-(\chi-\chi_0)^2/\delta\chi^2}$, where C is a normalization factor, then depending on the center, χ_0, and width, $\delta\chi$, of the Gaussian, a higher or lower percentage of beam ions might be trapped than the isotropic case would estimate.

This correction to the beam ion calculation could be significant, but it depends on the particular details of the neutral beams for the machine being considered. For NSTX, there are three separate beam sources, with possibly different energies, each having distinct full, half, and one-third energy components, and each can deposit particles on a particular surface at two different χ_0 angles (on the outboard and inboard sides of the surface). Efforts are underway to precisely model the anisotropic energetic particle distribution function
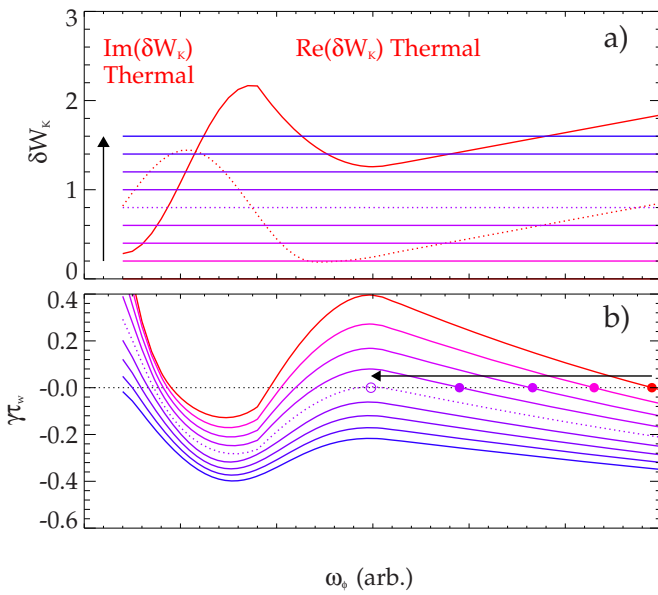
FIG. 9. (Color online) An illustrative example of the effect of energetic particle content on the marginal plasma rotation. The different curves denote increasing energetic particle content [upward in frame (a) and downward in frame (b)].
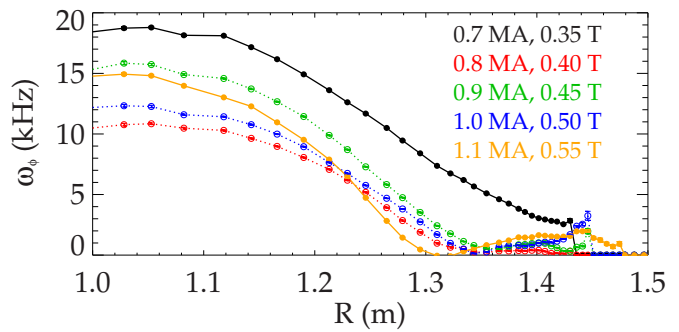

FIG. 10. (Color online) Plasma toroidal rotation profiles measured with CHERS (for carbon ions) for multiple NSTX discharges at the time of RWM instability.

as computed by "TRANSP" for NSTX as a linear combination of such Gaussian forms.

For now, a test of the role of anisotropy is performed by considering the simpler anisotropy model with constants $\chi_0(\Psi)=0.75$ and $\delta\chi(\varepsilon,\Psi)=0.25$, which puts a lower percentage of particles in the trapped range of χ around zero. This calculation has been included in Figs. 8(b) and 8(d). As expected, the lower trapped fraction leads to lower stability than the isotropic case (roughly half as much for this simple example). While this improved physics model of the energetic particle distribution moves the result closer to the experimental result, this change alone is not sufficient to bring quantitative agreement between the experimental observation of an unstable RWM and the calculated growth rate. Further improvements to the MISK model are presently being tested to explain the small difference in the growth rate ($\Delta\gamma\tau_w$ = 0.15–0.35) to bring the model to marginal stability. These will be discussed in Sec. V.

Besides the quantitative magnitude of γ, another important comparison between the model and the experiment is to examine the effect of energetic particles on the plasma rotation for marginal stability. Figure 9 shows an illustrative example in which representative Re(δW_K) and Im(δW_K) terms are made smaller than in Fig. 8(a), so that without energetic particles, the example plasma is unstable over a wider range of ω_ϕ. One can see that if plasma rotation is decreasing during a shot, it will reach the point of marginal stability at a relatively high level if the energetic particle pressure is low. As the pressure of the energetic particles is increased [modeled here by constant Re(δW) in Fig. 9(a)], the effect is to reduce the plasma rotation level necessary for stability (see arrows in the figure).

For the NSTX discharges shown in Fig. 7, the rotation profiles at the time of RWM instability are plotted in Fig. 10. When looking at the extremes (the solid lines), a clear dif-

ference between higher rotation at the lowest energetic particle content and lower rotation at the highest energetic particle content is evident. This is also true for the intermediate I_p values (with the exception of I_p=0.8 MA) if ω_ϕ is considered at $R\approx 1.3$ m, where it is changed most. However, a simple monotonic decrease was not obtained for all points across the entire ω_ϕ profile. This is most likely due to the sensitivity of stability to the evolution of plasma parameters and the change of the decreasing plasma rotation profile with time.

The physical model presented here for RWM stabilization can therefore represent NSTX experimental results qualitatively. In addition, as illustrated in Fig. 9, quantitative agreement would be produced if further improvements of the physics model yield a modest increase in $\gamma\tau_w$ from thermal particles. The experimental changes in energetic particle content have an effect on the marginal rotation, but they are not enough to push these NSTX plasmas from the upper (unstable) region of Fig. 9 fully into the lower (stable) region. This model is also consistent with DIII-D experiments where the energetic particle content is higher than in NSTX, and although the RWM growth rate is altered by changing plasma rotation, the plasma remains stable to the RWM, which would indicate that DIII-D plasmas are fully into the blue region of Fig. 9(b).

V. ASSESSMENT OF QUANTITATIVE AGREEMENT BETWEEN THE MODEL AND EXPERIMENT

The addition of isotropic energetic particles to the kinetic stability calculation for RWMs in NSTX has lead to results that are qualitatively consistent with experimental observation but farther from a quantitative match. Figures 8(b) and 8(d) show that the predicted $\gamma\tau_w$ at $\omega_\phi/\omega_\phi^{\text{expt}}$ is negative (−0.28 and −0.52), while in the experiment the RWM goes unstable at these rotation levels. These results can be considered to be not too far from agreement, however, since the mismatch is on the same order as the change in stability by slightly increasing or decreasing the plasma rotation. In the following subsections, we will first discuss three possible factors in moving toward a quantitative match between MISK calculations and experiments: the perturbative nature of the calculation, the sensitivity of the calculation to inputs, and
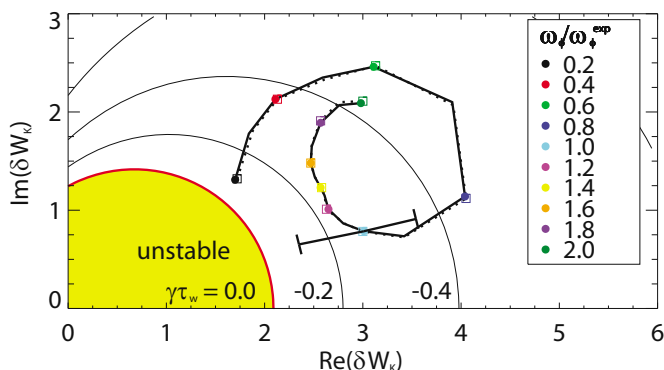
FIG. 11. (Color online) Stability diagram for NSTX shot 121083 @ 0.475 s. The solid line and points are the perturbative calculation, while the dashed line and open markers are for the iterated nonlinear inclusion of γ and ω_r.

the zero banana width approximation. Finally, further possible changes to the physical model will be discussed.

A. Perturbative versus self-consistent approaches

The MISK code takes a perturbative approach that differs from the self-consistent MARS-K code.[38] There are two main differences between the two approaches:[38] whether the RWM eigenfunction ξ is changed or unchanged by the kinetic effects and whether γ and ω_r are nonlinearly calculated.

First, the self-consistent approach calculates the RWM eigenfunction along with the kinetic calculation, while the perturbative approach assumes that the marginally stable ξ is unchanged. There is reason to believe that the kinetic effects of thermal particles have very little impact on ξ, from comparisons of fluid and self-consistent RWM eigenfunctions for DIII-D (Ref. 38) and ITER (Ref. 33) equilibria. However, it is possible that the kinetic effects of energetic particles could change ξ somewhat.[16]

Second, the RWM growth rate and real rotation frequency appear on both sides of the dispersion relation in Eq. (2) (since they appear on the right side in δW_K). In practice, when running MISK, γ and ω_r are usually set to zero in the equation for δW_K since they are small compared to other frequencies of the problem. However, it is also possible to iterate the calculated values of γ and ω_r from the left-hand side of Eq. (2) back into the right-hand side until convergence is reached. To do this, a value of $\tau_w = 5$ ms (a typical global scalar wall time from the 3D "VALEN" code) is used. Note that this time is representative of the RWM inverse growth time in experiments ($\gamma_{RWM}^{-1} = 6$ ms in Fig. 2). We have performed such an iteration for each calculation point (including isotropic energetic particles) in a scan of the scaled experimental rotation profile (characterized by $\omega_\phi / \omega_\phi^{exp}$). Figure 11 shows a reproduction of that calculation on a stability diagram of $Im(\delta W_K)$ versus $Re(\delta W_K)$. Contours of constant $\gamma \tau_w$, which are calculated by Eq. (2), form circular arcs on this diagram. In the shaded region, $\gamma > 0$ and the code predicts instability. The solid line and points are the original calculation, while the results of the iterated nonlinear inclusion of γ and ω_r are shown by the dashed line and open symbols. The change is negligible.

B. Sensitivity of the code to inputs

Figure 11 also gives a rough indication of the effect of errors in measured quantities on the calculation. For example, if the measured ω_ϕ was off by 10%, the result would shift along the plotted line to $\omega_\phi / \omega_\phi^{exp} = 0.9$ or 1.1. Uncertainties in the code calculation, meanwhile, manifest themselves as shifts in the locations of the points in Fig. 11. For example, a significant sensitivity in the calculation is the width of the Alfvén layers, Δq. A value of $\Delta q = 0.2$ was chosen as the smallest value that consistently eliminates issues in the numerical calculation.[9] A value of $\Delta q = 0.25$ eliminates more surfaces than necessary, which reduces δW_K and increases $\gamma \tau_w$, while $\Delta q = 0.15$ brings numerical error into the calculation from near the rational surfaces, reducing $\gamma \tau_w$. This range of $\Delta q = 0.15 - 0.25$ is indicated by the projected range of $\gamma \tau_w$ from -0.37 to -0.12 for the "1.0" point in Fig. 11. Sensitivities of the code calculation of this order are close but not large enough to explain the quantitative difference between the theoretical prediction including isotropic energetic particles and the experimental marginal point.

C. Zero banana width approximation

Another limitation of the present approach is that MISK uses a zero banana width approximation, i.e., the orbits of particles are considered to be confined into a single surface in Ψ. This approximation is used for thermal particles and has been previously validated by the benchmarking of "MARS" results (which make the same approximation) to results from the "HAGIS" code (which does not).[24,38]

It has not been investigated yet what effect this approximation has on the resulting energetic particle δW_K in NSTX. However, since the RWM is a global mode, not localized to particular surfaces like a toroidal Alfvén eigenmode, the effect of the thin orbit approximation may be minimal since particles that stray from their surfaces experience the mode in much the same way as those that do not.

Recently, it has been shown that accounting for the excursion of circulating anisotropic energetic particles away from single Ψ surfaces leads to an additional term in δW_K that can be destabilizing.[39] Currently, MISK does not include these factors (circulating particles, Ψ excursion, and correct χ asymmetry), but they are being considered to determine the importance of this theorized effect for NSTX.

D. Possible further changes to the physical model

Kinetic stability of the RWM calculated by MISK for NSTX equilibria, with isotropic energetic particles included, qualitatively captures the dependence of stability on plasma rotation seen in experiments but quantitatively overestimates that stability by an amount comparable to the variation of $\gamma \tau_w$ due to rotation effects. Altogether, we believe that if the eigenfunction does not change much and τ_w is not extraordinarily low, the differences between the perturbative and self-consistent approaches should be minor. However, a comparison between the self-consistent and the perturbative approaches for a DIII-D equilibrium including energetic particles, with the MARS-K code, does show major differences

between the approaches,[16] so the issue remains unresolved. The sensitivity of the code to input parameters does not seem to be able to fully explain the quantitative difference. Here, we describe other possible reasons for the discrepancy and work to improve the model toward quantitative agreement and predictive capability.

First is an improved model of the anisotropic distribution of beam ions, as described in the previous section. In addition to this, special attention must also be paid to the theoretical formulation of Eq. (4), as the combination of high beta and an anisotropic distribution function leads to an important additional term to $\tilde{f}$: $-\mu(\widetilde{B}_\parallel/B)(\partial f/\partial\mu)$.

Improvements to the theory of RWM stabilization in general and the thermal particle portion specifically are also possible. For example, the perturbative approach utilizes the dispersion relation in Eq. (2) that neglects plasma inertia. In the future, we plan to include this term, which could be important in high rotation plasmas. We have also neglected the electrostatic contribution[13] to δW_K, which is always a destabilizing effect, and may be significant for NSTX. Finally, the collision frequency in Eq. (4) is energy dependent, but not pitch angle dependent; a Lorentz collision operator could be used.

VI. CONCLUSION

Plasma rotation and energetic particles are known to have important effects on the stability of MHD modes in tokamaks. Within the framework of kinetic stability theory of resistive wall modes, an expression for δW_K in terms of the distribution function of the particles being considered was developed. An isotropic slowing-down distribution function was used in MISK code calculations of δW_K for alpha particles and for beam ions. For both alpha particles in ITER and beam ions in NSTX, predicted energetic particle stabilization is roughly in proportion to $\beta_a/\beta_{\text{tot}}$ and nearly independent of plasma rotation, so the nature of the thermal particle resonances is not affected by including energetic particles. Finally, the use of the perturbative approach and sensitivities to inputs are shown to be unlikely sources of quantitative discrepancy between the calculation and the experiment. However, as results including energetic particle effects are not far from quantitative agreement with experiment, consideration of terms previously considered to be small in the theory may bring close agreement with the high-beta plasmas presently under consideration in NSTX.

[1] A. Bondeson and D. Ward, Phys. Rev. Lett. **72**, 2709 (1994).
[2] E. Strait, T. Taylor, A. Turnbull, J. Ferron, L. Lao, B. Rice, O. Sauter, S. Thompson, and D. Wroblewski, Phys. Rev. Lett. **74**, 2483 (1995).
[3] S. Sabbagh, A. Sontag, J. Bialek, D. Gates, A. Glasser, J. Menard, W. Zhu, M. Bell, R. Bell, A. Bondeson, C. Bush, J. Callen, M. Chu, C. Hegna, S. Kaye, L. Lao, B. LeBlanc, Y. Liu, R. Maingi, D. Mueller, K. Shaing, D. Stutman, K. Tritz, and C. Zhang, Nucl. Fusion **46**, 635 (2006).
[4] R. Fitzpatrick and A. Aydemir, Nucl. Fusion **36**, 11 (1996).
[5] H. Reimerdes, T. Hender, S. Sabbagh, J. Bialek, M. Chu, A. Garofalo, M. Gryaznevich, D. Howell, G. Jackson, R. La Haye, Y. Liu, J. Menard, G. Navratil, M. Okabayashi, S. Pinches, A. Sontag, E. Strait, W. Zhu, M. Bigi, M. de Baar, P. de Vries, D. Gates, P. Gohil, R. Goebner, D. Mueller, R. Raman, J. Scoville, W. Solomon, DIII-D Team, JET-EFDA Contributors, and NSTX Team, Phys. Plasmas **13**, 056107 (2006).
[6] A. Garofalo, G. Jackson, R. La Haye, M. Okabayashi, H. Reimerdes, E. Strait, J. Ferron, R. Groebner, Y. In, M. Lanctot, G. Matsunaga, G. Navratil, W. Solomon, H. Takahashi, M. Takeshi, and A. Turnbull, Nucl. Fusion **47**, 1121 (2007).
[7] M. Ono, S. Kaye, Y. Peng, G. Barnes, W. Blanchard, M. Carter, J. Chrzanowski, L. Dudek, R. Ewig, D. Gates, R. Hatcher, T. Jarboe, S. Jardin, D. Johnson, R. Kaita, M. Kalish, C. Kessel, H. Kugel, R. Maingi, R. Majeski, J. Manickam, B. McCormack, J. Menard, D. Mueller, B. Nelson, B. Nelson, C. Neumeyer, G. Oliaro, F. Paoletti, R. Parsells, E. Perry, N. Pomphrey, S. Ramakrishnan, R. Raman, G. Rewoldt, J. Robinson, A. Roquemore, P. Ryan, S. Sabbash, D. Swain, E. Synakowski, M. Viola, M. Williams, and J. Wilson, Nucl. Fusion **40**, 557 (2000).
[8] S. Sabbagh, J. Berkery, R. Bell, J. Bialek, S. Gerhardt, J. Menard, R. Betti, D. Gates, B. Hu, O. Katsuro-Hopkins, B. LeBlanc, F. Levinton, J. Manickam, K. Tritz, and H. Yuh, Nucl. Fusion **50**, 025020 (2010).
[9] J. Berkery, S. Sabbagh, R. Betti, B. Hu, R. Bell, S. Gerhardt, J. Manickam, and K. Tritz, Phys. Rev. Lett. **104**, 035003 (2010).
[10] W. Zhu, S. Sabbagh, R. Bell, M. Bell, B. LeBlanc, S. Kaye, F. Levinton, J. Menard, K. Shaing, A. Sontag, and H. Yuh, Phys. Rev. Lett. **96**, 225002 (2006).
[11] J. Jacquinot and S. Putvinski, Nucl. Fusion **39**, 2471 (1999).
[12] I. Chapman, V. Igochine, J. Graves, S. Pinches, A. Gude, I. Jenkins, M. Maraschek, and G. Tardini, Nucl. Fusion **49**, 035006 (2009).
[13] B. Hu, R. Betti, and J. Manickam, Phys. Plasmas **12**, 057301 (2005).
[14] B. Hu, R. Betti, and J. Manickam, Phys. Plasmas **13**, 112505 (2006).
[15] R. Aymar, V. Chuyanov, M. Huguet, and Y. Shimomura, Nucl. Fusion **41**, 1301 (2001).
[16] Y. Liu, M. Chu, W. Guo, F. Villone, R. Albanese, G. Ambrosino, M. Baruzzo, T. Bolzonella, I. Chapman, A. Garofalo, C. Gimblett, R. Hastie, T. Hender, G. Jackson, R. La Haye, M. Lanctot, Y. In, G. Marchiori, M. Okabayashi, R. Paccagnella, M. Furno Palumbo, A. Pironti, H. Reimerdes, G. Rubinacci, A. Soppelsa, E. Strait, S. Ventre, and D. Yadykin, "Resistive wall mode control code maturity," Plasma Phys. Controlled Fusion (to be published).
[17] G. Matsunaga, N. Aiba, K. Shinohara, Y. Sakamoto, A. Isayama, T. Takechi, T. Suzuki, N. Oyama, N. Asakura, Y. Kamada, and T. Ozeki, Phys. Rev. Lett. **103**, 045001 (2009).
[18] N. Gorelenkov, M. Van Zeeland, H. Berk, N. Crocker, D. Darrow, E. Fredrickson, G. Fu, W. Heidbrink, J. Menard, and R. Nazikian, Phys. Plasmas **16**, 056107 (2009).
[19] S. Sabbagh, R. Bell, M. Bell, J. Bialek, A. Glasser, B. LeBlanc, J. Menard, F. Paoletti, D. Stutman, E. Fredrickson, A. Garofalo, D. Gates, S. Kaye, L. Lao, R. Maingi, D. Mueller, G. Navratil, M. Ono, M. Peng, E. Synakowski, and W. Zhu, Phys. Plasmas **9**, 2085 (2002).
[20] S. Sabbagh, R. Bell, J. Menard, D. Gates, A. Sontag, J. Bialek, B. LeBlanc, F. Levinton, K. Tritz, and H. Yuh, Phys. Rev. Lett. **97**, 045004 (2006).
[21] S. Haney and J. Freidberg, Phys. Fluids B **1**, 1637 (1989).
[22] M. Chu, J. Greene, T. Jensen, R. Miller, A. Bondeson, R. Johnson, and M. Mauel, Phys. Plasmas **2**, 2236 (1995).
[23] B. Hu and R. Betti, Phys. Rev. Lett. **93**, 105002 (2004).
[24] Y. Liu, M. Chu, I. Chapman, and T. Hender, Phys. Plasmas **15**, 112503 (2008).
[25] J. Van Dam, M. Rosenbluth, and Y. Lee, Phys. Fluids **25**, 1349 (1982).
[26] F. Porcelli, Plasma Phys. Controlled Fusion **33**, 1601 (1991).
[27] J. Graves, R. Hastie, and K. Hopcraft, Plasma Phys. Controlled Fusion **42**, 1049 (2000).
[28] J. Graves, I. Chapman, S. Coda, T. Johnson, M. Lennholm, B. Alper, M. de Baar, K. Crombe, L. Eriksson, R. Felton, D. Howell, V. Kiptily, H. Koslowski, I. Mayoral, I. Monakhov, I. Nunes, and S. Pinches, Nucl. Fusion **50**, 052002 (2010).
[29] Y. Liu (private communication).
[30] R. Budny, M. Bell, H. Biglari, M. Bitter, C. Bush, C. Cheng, E. Fredrickson, B. Grek, K. Hill, H. Hsuan, A. Janos, D. Jassby, D. Johnson, L. Johnson, B. Leblanc, D. McCune, D. Mikkelsen, H. Park, A. Ramsey, S. Sabbagh, S. Scott, J. Schivell, J. Strachan, B. Stratton, E. Synakowski, G. Taylor, M. Zarnstorff, and S. Zweben, Nucl. Fusion **32**, 429 (1992).
[31] S. Sabbagh, S. Kaye, J. Menard, F. Paoletti, M. Bell, R. Bell, J. Bialek, M.

Bitter, E. Fredrickson, D. Gates, A. Glasser, H. Kugel, L. Lao, B. LeBlanc, R. Maingi, R. Maqueda, E. Mazzucato, D. Mueller, M. Ono, S. Paul, M. Peng, C. Skinner, D. Stutman, G. Wurden, W. Zhu, and NSTX Research Team, Nucl. Fusion **41**, 1601 (2001).

[32]R. Grimm, J. Greene, and J. Johnson, *Methods in Computational Physics* (Academic, New York, 1976), Vol. 16, pp. 253–280.

[33]Y. Liu, M. Chu, I. Chapman, and T. Hender, Nucl. Fusion **49**, 035004 (2009).

[34]A. Polevoi, S. Medvedev, V. Pustovitov, V. Mukhovatov, M. Shimada, A. Ivanov, Y. Poshekhonov, and M. Chu, *Proceedings of the 19th IAEA Fusion Energy Conference*, Lyon, France (International Atomic Energy Agency, Vienna, 2002), Vol. 1, Paper No. CT/P–08.

[35]N. Gorelenkov, H. Berk, and R. Budny, Nucl. Fusion **45**, 226 (2005).

[36]M. Podestà, W. Heidbrink, R. Bell, and R. Feder, Rev. Sci. Instrum. **79**, 10E521 (2008).

[37]I. Chapman, S. Pinches, L. Appel, R. Hastie, T. Hender, S. Saarelma, S. Sharapov, I. Voisekhovitch, and J. Graves, Phys. Plasmas **14**, 070703 (2007).

[38]Y. Liu, I. Chapman, M. Chu, H. Reimerdes, F. Villone, R. Albanese, G. Ambrosino, A. Garofalo, C. Gimblett, R. Hastie, T. Hender, G. Jackson, R. L. Haye, M. Okabayashi, A. Pironti, A. Portone, G. Rubinacci, and E. Strait, Phys. Plasmas **16**, 056113 (2009).

[39]J. Graves, I. Chapman, S. Coda, L. Eriksson, and T. Johnson, Phys. Rev. Lett. **102**, 065005 (2009).